Transient events in the EUV transition region and chromosphere

P.T. Gallagher[1,2], **K.J.H. Phillips**[2], **L.K. Harra-Murnion**[3], **F. Baudin**[4], and **F.P. Keenan**[1]

[1] Department of Pure and Applied Physics, The Queen's University of Belfast, Belfast, BT7 1NN, Ireland
[2] Space Science Department, Rutherford Appleton Laboratory, Chilton, Didcot, Oxon. OX11 0QX, UK
[3] Mullard Space Science Laboratory, Holmbury St Mary, Dorking, Surrey RH5 6NT, UK
[4] Institut d'Astrophysique Spatiale, Université Paris XI-CNRS, Bât. 121, F-91405 Orsay Cedex, France

Abstract. Rapid time cadence observations of the quiet Sun extreme ultraviolet emission, observed by the CDS instrument on SOHO, are discussed. Numerous transient brightenings are observed in network features in both a transition region line (O V 629.73 Å) and a chromospheric line (He I 584.33 Å), indicating a dynamic coupling between the chromospheric and transition region network. Their durations are between 80 and 200 s and dimensions 6 000–10 000 km. A wavelet analysis reveals a tendency for semi-periodic behaviour, with excess power at a frequency of about 4 mHz. The variations are much less evident in the internetwork or cell regions, although they are again semi-periodic. Relative line-of-sight velocities have also been derived from the data, the CDS spectral resolution allowing a precision of between 4.7 and 6 km s^{-1}. There is a clear association of brightenings in the network with downflows of $\sim$ 13 km s^{-1} at 250 000 K with some events having velocities of up to $\sim$ 20 km s^{-1}, these being measured relative to the average quiet Sun emission. Within the internetwork, we also find a weak correlation between events seen in the He I (584.33 Å) and the O V (629.73 Å) lines. In this case, the events have a smaller size ($\leq$ 2 000 km), amplitude (both in terms of their intensity and velocity), and also show a higher frequency of about 6 mHz.

The apparent differing properties of network and internetwork events implies that both these regions are heated by two distinct mechanisms. In the case of the internetwork, these results further confirm that acoustic waves propagating up from the photosphere and forming shocks in the overlying atmosphere are the most likely heating mechanism. For the network, it is apparent that the heating required must be in excess of that supplied by acoustic shocks. Our view is that the network events are produced by nanoflare-like magnetic reconnections in the corona, or possibly excitation due to a spicule-type event in which there is a repeated rebound.

Key words: Sun: UV radiation – Sun: chromosphere – Sun: transition region – Sun: corona

1. Introduction

It has been known for many years (Dere et al., 1983, Porter et al., 1987) that the ultraviolet emission from the transition region is highly variable, and particular features of the network show large velocity shifts towards and away from the observer. These facts have been confirmed with observations from the *Solar and Heliospheric Observatory* (SOHO) spacecraft, and recent analysis has emphasized the significance of the observations for understanding the heating mechanism of the solar chromosphere and corona, which remains one of the unsolved mysteries of solar physics (see Ulmschneider et al., 1991). It appears that the lower internetwork chromosphere is heated by dissipation of non-magnetic acoustic shocks (Carlsson et al., 1997, Carlsson & Stein, 1997, Doyle et al., 1999). However it is likely that a large number of small-scale magnetic reconnections (Schrijver et al., 1998) which may be associated with events seen in extreme ultraviolet (EUV) and X-ray emission (Harrison, 1997, Berghmans et al., 1998, Preś & Phillips, 1999), are involved in the heating of the chromosphere and transition region in network regions, located at the edges of photospheric supergranules.

The variable nature of the EUV transition region is particularly evident in observations of the quiet-Sun taken during the recent solar minimum with the Coronal Diagnostic Spectrometer (CDS) on SOHO (Harrison et al., 1995). In this paper we report on transient EUV events within the network and in particular the downflows which we find associated with them. The brightenings have been observed in emission lines due to He I and O V and as the electron temperature T_e of maximum emissivity for these ions is $\log(T_e) = 4.5$ and 5.4 respectively, so He I can be regarded as chromospherically formed, while O V is a transition region ion. The temperature of formation of O V was estimated from the peak of the contribution function obtained from the Atomic Data and Analysis Structure (ADAS) package (Summers 1994). The He I formation temperature was calculated from the ion fractions of Arnaud & Rothenflug (1985) and excitation rate coefficients, approximated by $\exp(-W/kT_e)/T_e^{1/2}$ where W is the excitation energy. It should also be noted that estimating a specific He I formation temperature is somewhat complicated by the fact that the contribution function is not strongly peaked in temperature (see Gallagher et al., 1998). This is probably due to the fact that He I transitions are not solely excited by collisional

Table 1. Details of the NTBRMDI observing sequences.

Instrument	CDS/NIS	
Slit size used	$4'' \times 240''$	
Ions	He I (584.33 Å $\pm$2.7 Å)	
	O V (629.73 Å $\pm$2.7 Å)	
Exposure time	15 s	
	NTBRMDI1	NTBRMDI2
Area	$240'' \times 240''$	$4'' \times 240''$
No. of exposures	60	360
Duration (mins)	15	90

processes but are though to be excited by other mechanisms such as the photoionization-recombiation process (Andretta & Jones, 1997, Athay, 1988).

This paper describes the high cadence observations that were planned for this work (Sect. 2) and the methods used to reduce and analyze the data (Sect. 3). In Sect. 4 we report on the dynamic nature of network and cell regions, and in particular on the association of O V and He I line intensities and velocities. We discuss how these observations can be interpreted in light of recent theoretical studies in Sect. 5, in particular models involving spicule rebound and nano-flares in the corona.

2. Observations

The SOHO/CDS instrument consists of the Normal Incidence Spectrometer (NIS) and Grazing Incidence Spectrometer (GIS) operating in the EUV spectral region, both having the capability of forming images at particular spectral lines. The NIS used for the current observations is a stigmatic spectrometer with a long entrance slit, with images being formed by moving the solar image across the slit by a scan mirror. The spectral ranges of the NIS (308–381 Å, 513–633 Å) include lines that are formed over a large temperature range (approximately 10^4 to 10^6 K), so that images of the Sun can be formed simultaneously which extend from the upper chromosphere through the transition region to the corona.

A quiet region of the Sun near disc centre was observed with the NIS between 12:53 U.T. and 15:16 U.T. on 1996 December 19 using a sequence called NTBRMDI, which we designed specially for following rapid variations of the EUV flux. Table 1 gives the details of this sequence. A context image of size $4' \times 4'$ (NTBRMDI1) was first performed at Sun centre using the $4'' \times 240''$ slit with a narrow (5.4 Å) spectral window centred on the He I and O V lines at 584.33 Å and 629.73 Å respectively, taking approximately 20 minutes (see Fig. 1). A 90-minute-long time-series of slit images (NTBRMDI2) was then made using the $4'' \times 240''$ slit (longer dimension in a north–south or Solar_Y direction). A set of 360 such images, each taking 15 s, was obtained. These slit images were centred on a position that was constant with reference to the solar image, with solar feature tracking turned off. As a consequence, solar features were free to move into and out of the slit field of view by solar rotation, although the motion is at the slow rate of $9''$ per hour. In previous work (Gallagher et al., 1998) we found that the typi-
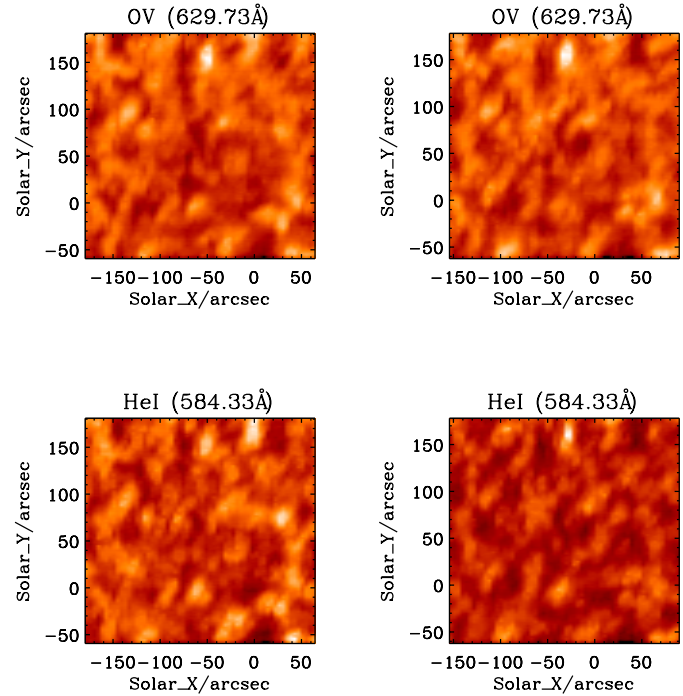

Fig. 1. The quiet Sun EUV network in O V (629.73 Å) and He I (584.33 Å) on 1996 December 19. The rasters on the left were taken at 12:53 U.T., those on the right at 15:16 U.T. (start times). Although there are minor changes in this period, the large-scale structures remain unchanged.

cal dimension of network features seen with CDS was $\sim 10''$, so that any variations in the intensity recorded in times much faster than an hour are likely to be true variations and not due to emission features passing the field of view. Recently, EUV Images produced using SUMER and TRACE have identified features down to $1''$ which are unobservable with CDS due to the instruments reduced spatial resolution. Finally, a further $4' \times 4'$ context image (NTBRMDI1) was taken to examine any changes that occurred in the region of interest.

3. Data analysis

Using standard CDS software, the data were first corrected for cosmic ray events and CCD readout bias, and flat-fielded before the final calibration step was performed to convert the raw data in Analogue to Digital Conversion units (ADC) into absolute units (photons cm^{-2} s^{-1} arcsec^{-2}). A further correction, allowing for the fact that the dispersion axes of the NIS spectra are slanted relative to the CCD detector (x,y) axes, was applied using standard CDS tilt-correction routines.

The profiles of the He I and O V spectral lines were then extracted from each pixel in both the NTBRMDI1 and NTBRMDI2 sequences and the line intensity and position were estimated from Gaussian fits to the spectrum as described by Gallagher et al. (1998). As an absolute wavelength calibration has not yet been applied to CDS spectral data, we chose to measure any wavelength shift due to mass flows relative to the average position of each line observed in the $4' \times 4'$ context rasters taken
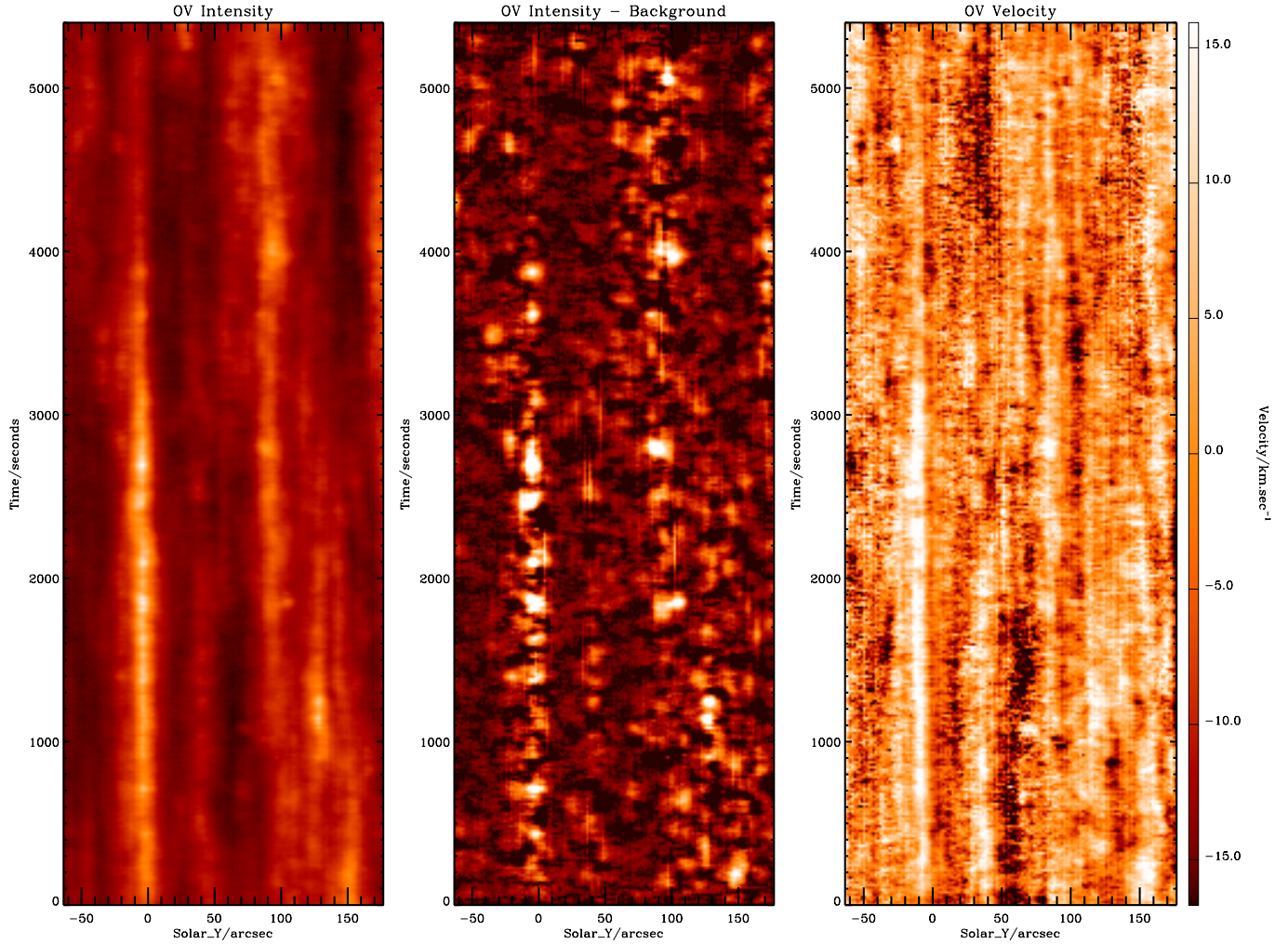
Fig. 2. Line intensity (*left panel*), line intensity after background subtraction (*middle panel*) and velocity (*right panel*) 'space-time' plots for the transition region O V ion. The abscissa gives position along the slit in arcseconds while the ordinate displays the time in seconds. In the velocity figure, light areas correspond to positive values, i.e. red shifts (the magnitude of the velocity is indicated by the vertical bar to the right of the figure).

directly before and after the NTBRMDI2 sequence. The position of each spectral line then defined the velocity v of the emitting material in each pixel through $v = c[(\lambda - \lambda_{\text{average}})/\lambda_{\text{average}}]$, where $(\lambda - \lambda_{\text{average}})$ is the wavelength shift compared with the average line position and c is the velocity of light. The uncertainty σ_λ in the determination of the line position was estimated using

$$\sigma_\lambda = \frac{\sigma}{\sqrt{N}} \tag{1}$$

where N is the total number of photon-events per pixel and σ is the standard deviation of the Gaussian fit.

The uncertainty in the velocities estimated from the He I line was thus found to be $\sim 4.7\,\text{km}\,\text{s}^{-1}$ while that in the O V line velocities was found to be $\sim 6\,\text{km}\,\text{s}^{-1}$. These uncertainties are however reduced by summing over several pixels in the Solar_Y direction. Note that in referencing our spectral data to the average wavelength in the context images, we disregard any wavelength shift of lines present in these averages. On the

Table 2. Characteristics of the $4' \times 4'$ average line profiles taken directly before and after the high cadence observations. The intensity is quoted in photons cm^{-2} s^{-1} arcsec^{-2} while all other values are in Å.

	Before		After	
	He I	O V	He I	O V
Intensity	144.876	115.809	143.682	115.462
Position	584.398	629.861	584.407	629.870
FWHM	0.53468	0.54174	0.53614	0.54282

basis of previous work (e.g. Teriaca et al. 1999, Achour et al. 1995), there is likely to be a small redshift corresponding to $\sim 2.5\,\text{km}\,\text{s}^{-1}$ and $\sim 7\,\text{km}\,\text{s}^{-1}$ at the formation temperatures of He I and O V respectively.

A further effect, which should be taken into account when calculating velocities is that which the CDS optical bench temperature has on the NIS wavelength zero-point. This is significant when the instrument has previously been pointed at off-
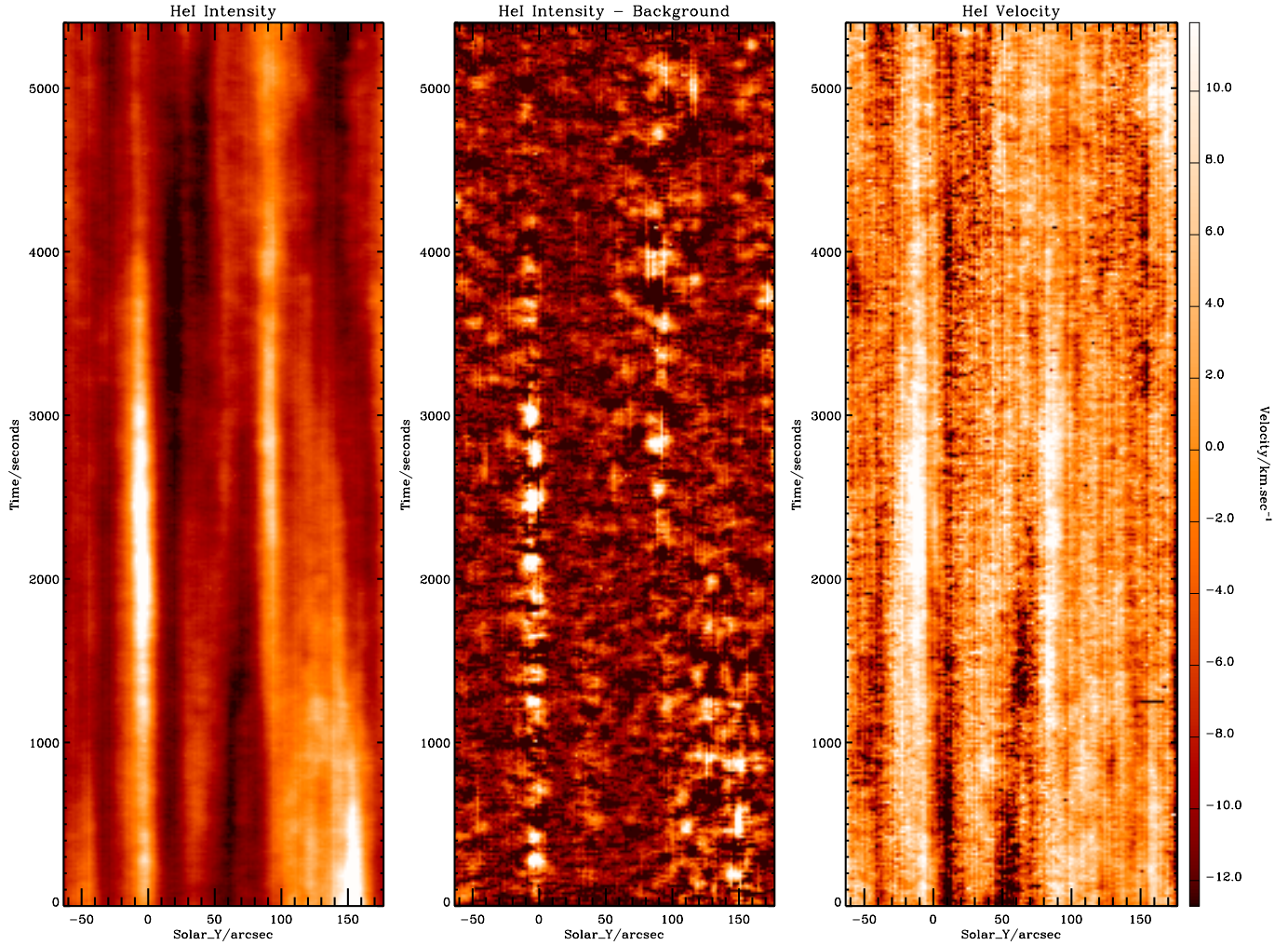
Fig. 3. Line intensity (*left panel*), line intensity after background subtraction (*middle panel*) and velocity (*right panel*) 'space-time' plots for the transition region He I ion. The abscissa gives position along the slit in arcseconds while the ordinate displays the time in seconds. The velocity scale is indicated by the vertical bar as in Fig. 2.

limb or active region locations. However, on this occasion the high-cadence observations were taken after almost 2 hours of continuous quiet Sun observations, which should be an adequate time for the optical bench to reach a stable temperature. To check this, the line profiles from the two NTBRMDI1 sequences were inspected. It was found that, in the 90-minute period between them, the lines were shifted by only 9 mÅ or less, which is of the same order as the error in line peak wavelength determination. See Table 2 for more details. Thus, we consider this effect to be negligible for the observations discussed here.

In the case of the intensity variations, a background level was removed from each light curve along the slit by identifying local minima along the curve and then fitting the selected points using a purpose-written linear interpolation routine. This background was then subtracted from the data.

4. Results

Fig. 1 shows the context ($4' \times 4'$) images in the He I and O V lines which were made at 13:00 U.T. and 15:26 U.T. (start times), i.e.

directly before and after the sequence of slit images. They show the bright structures in the form of a network, typical of the quiet Sun in the EUV, the properties of which have been described by Gallagher et al. (1998) and other authors. As mentioned, the He I image is appropriate to the solar chromosphere (peak emissivity temperature $T_e \sim 30\,000$ K), but the O V line is formed in the transition region ($T_e \sim 250\,000$ K). As discussed by Gallagher et al., the more structured appearance of the O V image is most likely due to the large optical depth of the He I line. As can be seen, the gross network features remain largely unchanged in the 90-minute interval between the two context images, as expected with the approximately one-day lifetime of supergranules, although some regions undergo brightness changes by the later time.

The output from the NTBRMDI2 slit images can be shown as a 'space–time' plot, in the left-hand panels of Fig. 2 for the O V and Fig. 3 for He I. In these plots, the solar north–south (Solar_Y) space direction is the horizontal axis, the vertical axis is time, with $t = 0$ at the foot of each plot. Vertical light streaks
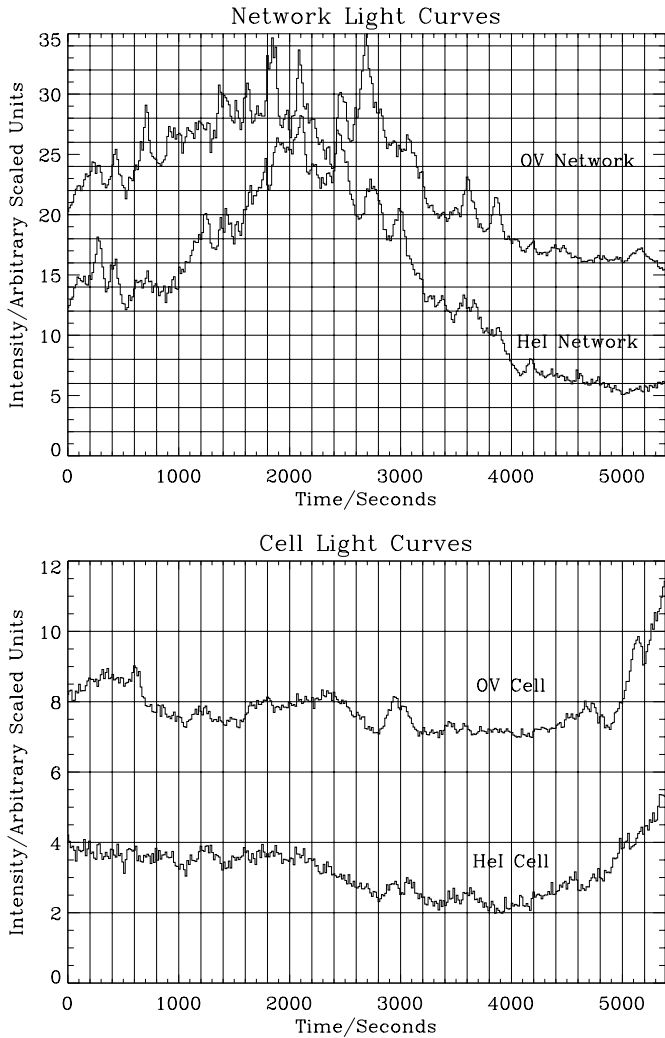
Fig. 4. Intensity variation (before background subtraction) as a function of time for a typical network (Solar_Y = -2″) and cell region (Solar_Y = 20″) in O V (629.73 Å) and He I (584.33 Å). The grid on these plots clearly shows that the times of peak emission are negligibly different between the two lines.

are the network emission features passing across the slit field of view. Superposed on these streaks are localized bright regions (dimensions about 8–15″, or 6 000–10 000 km) and lasting between about 80 and 200 s. These are real time variations in the emission since motion of bright features across the slit by solar rotation would result in much slower variations. Faint vertical streaks are either faint parts of the network or internetwork ('cell') structures. It is clear that the network features are highly variable in intensity, and that the variation is much less smooth for the O V line emission than for He I.

These variations can be seen much more clearly in the central panels of Figs. 2 and 3, in which the background intensity level is subtracted as described earlier. From these figures we can see some evidence for periodicity in the emission along one of the network features in both the O V and He I lines (Solar_Y = -2″), the frequency being about 4 mHz. We are in the pro-

cess of investigating this further using wavelet analysis, but a preliminary result is presented in Fig. 5 for a network feature. It appears that there is indeed excess power at some times during the 90-minute observing sequence at this and smaller frequencies. Further, within one of the cells (Solar_Y = 20″), there is excess power at around 6 mHz, and this can also just be seen in Figs. 2 and 3.

Our findings concerning the semi-periodic behaviour of the He I and O V line emission appear to be similar to those of Baudin et al. (1998) from optical observations made with the Richard B. Dunn Telescope at the National Solar Observatory/Sacramento Peak. They observed velocity variations in the Ca II K and He I chromospheric lines, and found similar periods to ours for network and cell structures. Furthermore, recent work by Doyle et al. (1998) using CDS has also finds clear evidence for oscillations with periods of 3 to 5 mins in mid transition region lines such as O III, O IV, and O V.

We also derived line-of-sight velocities from the O V and He I spectra using the procedure discussed earlier. These are plotted as two-dimensional images in the right-hand panels of Figs. 2 and 3 respectively. In these plots, bright areas correspond to downward motions (red-shifted line emission), and dark areas to upward motions (blue-shifted line emission). There are several areas of enhanced emission in the network which are strongly correlated with downward motions of up to $\sim$ 20 km s^{-1} in both lines, examples of which can be seen at $t =$ 2800 s and 1850 s. Thus, brightenings are frequently correlated with downflows. We have attempted to do a wavelet analysis as with the intensities, but the uncertainties seem too large to make any definite conclusions at this point. This will be discussed in a future paper.

Such variations have been noted from observations made with the SUMER (Solar Ultraviolet Measurements of Emitted Radiation) instrument on SOHO (Judge, Carlsson, & Wilhelm 1997), who also note that transition region emission lines in the SUMER wavelength range are less smoothly varying than the He I 584 Å line. They attribute this at least in part to the longer recombination times one would expect for He ions (up to 300 s) than for transition region lines, so that in a recombining plasma the He spectrum reacts to changes in temperature in times equal to at least this period. In addition, there is the fact that the optical depth of the He I line is very large, so that sudden intensity increases are likely to be smeared by radiative transfer effects.

Fig. 4 shows light curves of particular features in O V and He I by summing over several pixels at Solar_Y = -2″ for the network emission and Solar_Y = 20″ for the internetwork emission. It is clear that the brightenings in the network feature are far more numerous and energetic than in the cell. This will be studied in a forthcoming work (Harra-Murnion et al., in preparation). It is also clear that brightenings in the O V emission are highly time-correlated with those in He I emission, with little evidence of appreciable differences in the peak times. This applies to both cell and network features.

Fig. 6 gives the intensity histograms along the slit for the O V emission (top panels), as well as the mean intensity ($\mu(I)$) and root mean square deviation ($\sigma(I)$) (bottom two panels). (Note
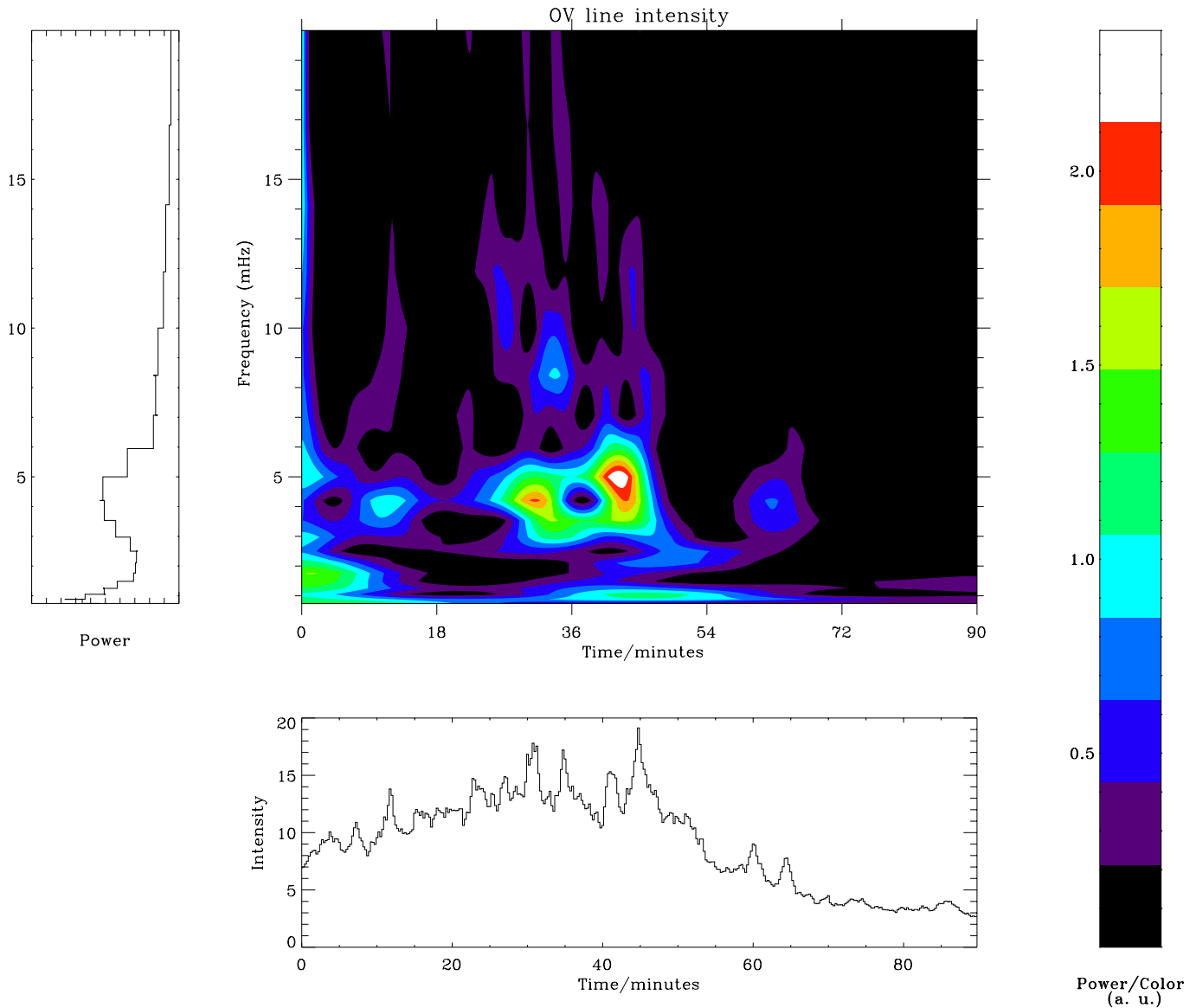
Fig. 5. Wavelet analysis for the O V network lightcurve. The central panel shows the time-frequency phase plane plot of the lightcurve given at bottom. Here, the brighter the region, the more energy is in that sample. The left-hand plot gives the standard Fourier transform of the lightcurve. There is repeated power seen at ~ 4 mHz during the 90 minute observation with some evidence for power above ~ 7 mHz.

that in the top panels the frequency of any particular intensity is indicated by the grey-scale vertical bar to the right.) It can be seen that the network regions produce comparatively high-intensity events compared with cell regions. The latter in fact do produce numerous low-intensity events ($\mu(I)$ less than about 2 photons cm^{-2} sec^{-1} $arcsec^{-2}$) in both lines, whereas this is not the case for the network (indicated by the presence of large number of low intensity values for the cell). Table 3 gives values of the mean and standard deviation in the network and cell intensities that illustrate the above points further.

Fig. 7 is a time plot of the relative velocity in network and cell regions for both the O V and He I lines. For the network, times of large positive velocities correspond in the majority of cases to times of intensity peaks (the intensities are also shown

in the figures, taken from Fig. 4). This supports the impression from Figs. 2 and 3 mentioned earlier. For the cell region, there is no obvious correlation between intensity and velocity, possibly indicating a different heating mechanism from the network region. We examined typical network and cell regions for any relation between line intensity and velocity (Figs. 8 and 9), finding a strong correlation for the network region in both the O V and He I lines but little or no relationship for the cell region. The correlation coefficient for the linear relationship between the network intensity and velocity was found to be ~ 0.82, implying again that a large number of events show both an intensity and a velocity signature.

A summary of our findings for the events seen in the network and cell regions is given in Table 3.
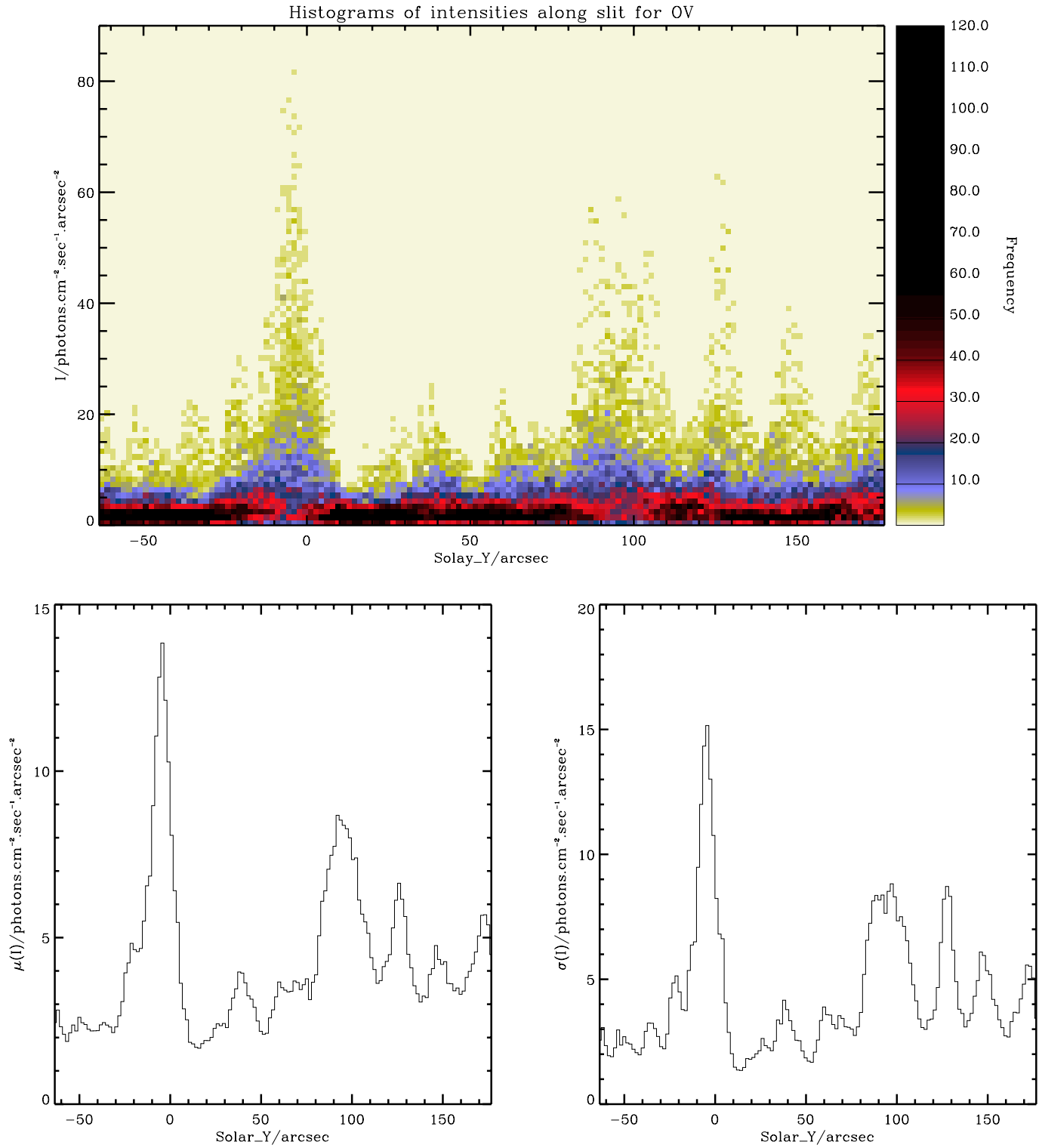
Fig. 6. The top panel gives a 2D representation of the distribution of intensities along the slit for O V transition region line formed at $\log(T_e) = 5.4$. (*Lower left:*) The mean intensity ($\mu(I)$) observed along the slit after background subtraction showing that the mean intensity of the brightenings is larger along the network. (*Lower right:*) The root mean square deviation ($\sigma(I)$) of the brightenings. Note the intensity and velocity curves in Figs. 4 and 7 are taken from Solar_Y = -2″ and Solar_Y = 20″.

Table 3. Characteristics of network and cell events (intensities in photons cm^{-2} s^{-1} arcsec^{-2} and velocities in km s^{-1}).

	Network	Cell
Mean ± RMS velocity[1] (O v)	13 ± 5	- 4 ± 4
(He i)	7 ± 3	- 3 ± 2
Mean ± RMS intensity (O v)	13.9 ± 15.1	2.20 ± 2.5
(He i)	11.2 ± 10.9	2.50 ± 1.9
Lifetimes	80–200 s	≤ 150 s
Spatial extent	∼ 7000 km	∼ 2000 km
Frequency	∼ 4 mHz	∼ 6 mHz
Period	∼ 4.2 min	∼ 2.7 min

[1] Measured relative to average quiet Sun velocity of ∼ 0 km s^{-1}

5. Discussion and conclusions

5.1. Network features

We have found strong evidence of pulse-like transient brightenings in the quiet-Sun network that are correlated with locations of red-shifted line emission in the He i and O v line emission. Further there is some evidence for periodic behaviour, with periods of ∼ 250 s. In the case of the optically thin O v line, it is also possible to assume that the line intensity is related to the local electron density through $I \sim N_e^2$, suggesting that the observed brightenings are produced via rapid compression of the transition region plasma.

The ubiquity of these events in these typical quiet-Sun data set would suggest a connection with a very frequent solar phenomenon driven by either pressure pulses or magnetic reconnection. As noted many times by other authors, red-shifted transition region line emission might be due to a number of reasons, e.g. siphon flows in loops (Mariska 1988, McClymont 1989), return of spicular material (Cheng 1992a, b, c, Hansteen & Wikstøl 1994) or nanoflare-related magnetic reconnection events (Hansteen et al. 1996), with models by the cited authors to explain the presence of line shifts. Furthermore, 5-min velocity and magnetic oscillations have been reported by Ulrich (1996) who attributed these events to magnetohydrodynamic oscillations with that properties of Alfvén waves.

Magnetic reconnection appears to be favoured by many authors, including those who have studied images and velocity data from the SUMER instrument on SOHO (Judge et al. 1998). Models (Hansteen et al. 1996) have been developed in which magnetohydrodynamic waves are generated by a magnetic reconnection or nanoflare event in the corona just above the network transition region which propagate downwards and give rise to a compression and heating of material. The net result is that transition region emission line profiles are red-shifted, with the bulk of the emitting gas flowing downwards. The reconnection does not lead to a repeated formation of a heated pulse, although several nanoflares may occur in the same region over a short time period (150 s was considered by Hansteen et al. 1996). Red-shifted velocities in transition region lines are expected to be several tens of km s^{-1}.

A widely accepted theory for spicule formation due to Hollweg (1982) and expanded upon by many other authors (e.g.
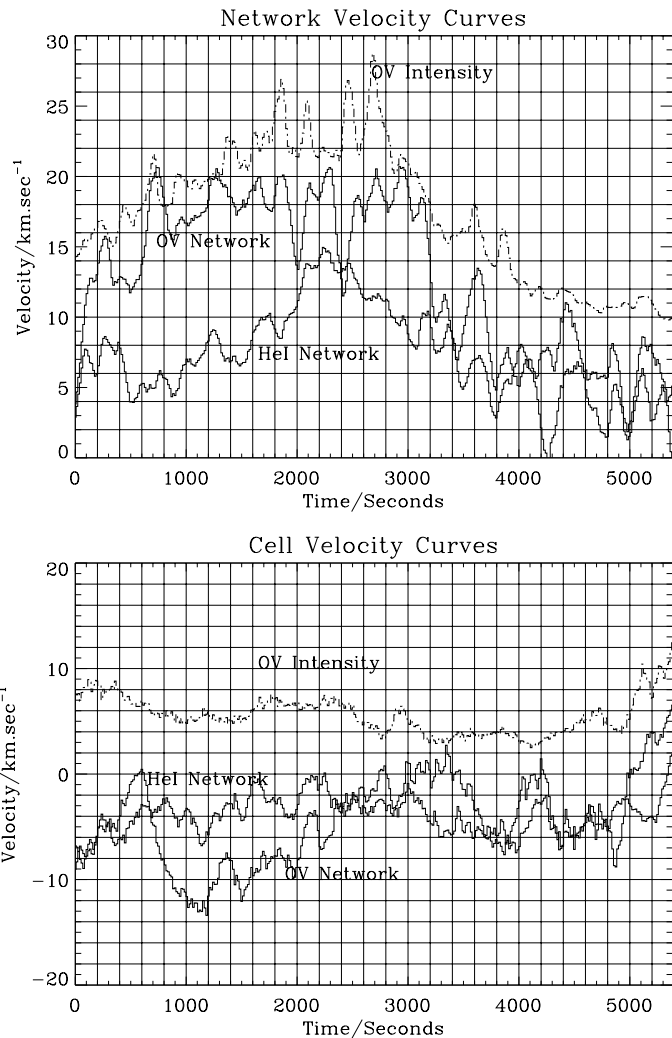

Fig. 7. Relative line-of-sight velocity variation as a function of time for a typical network and cell region in O v (629.73 Å) and He i (584.33 Å). The dotted line in the uppermost panel gives the O v line intensity curve for the same network region.

Sterling & Hollweg 1988; Sterling & Mariska 1990), is relevant to this discussion. The idea is based on the fact that a large mass is observed to be ejected by Hα spicules, about a factor 100 times more than the observed mass flux in the solar wind, so that there must be a return of the spicular material to the chromosphere. The hydrodynamic models of Cheng (1992a, b, c) and Hansteen & Wikstøl (1994), which agree remarkably well given the different boundary conditions, both predict a damped oscillation of material as the transition region is first lifted by the spicule, with material in the wake of the shock so formed falling and cooling. This causes a heating of the atmosphere below, which in turn leads to a further rise. A repeated pulse is thus formed, with material downflows having velocities of about 40 km s^{-1}. Hansteen & Wikstøl comment on the paradoxical fact that, in spite of the velocity downflows expected by their model, transition region lines such as the C IV lines at 1548, 1550 Å are expected to show strong *blue* shifts at the time of the first spicular pulse, followed by a drift to a red shift but
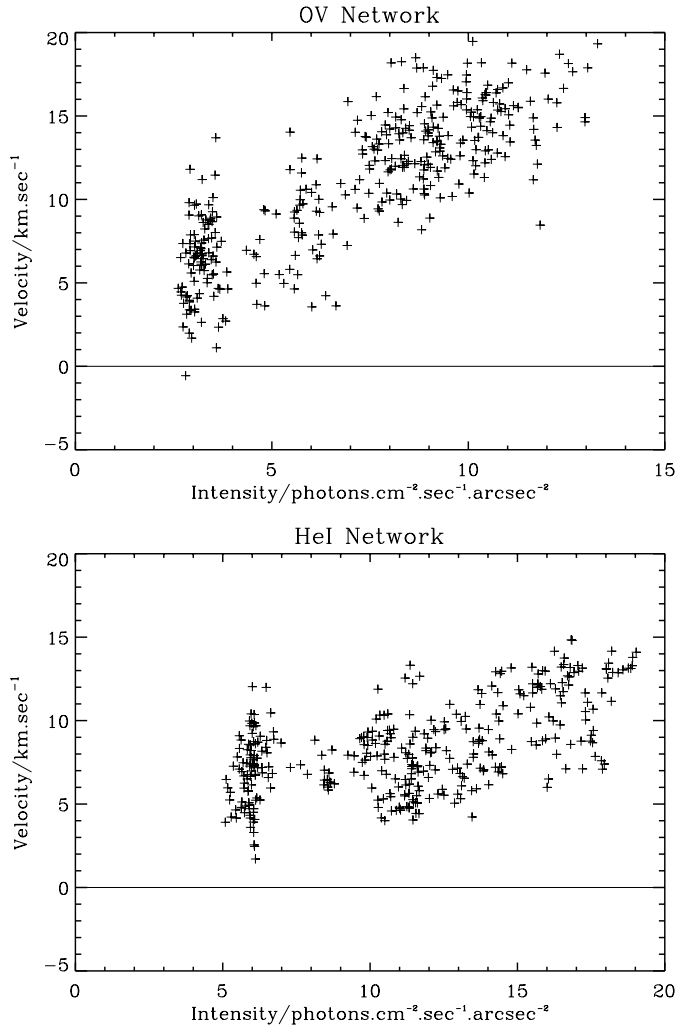
Fig. 8. Line of sight velocity in $km\,s^{-1}$ as a function of line intensity (photons $cm^{-2}\,s^{-1}$ $arcsec^{-2}$) for a typical *network* region. The upper panel shows a scatter plot for the O V ion while the corresponding He I relationship is given at bottom.

Fig. 9. Line of sight velocity in $km\,s^{-1}$ as a function of line intensity (photons $cm^{-2}\,s^{-1}$ $arcsec^{-2}$) for a typical *cell* region. The upper panel shows a scatter plot for the O V ion while the corresponding He I relationship is given at bottom.

with the line emission decreasing by this time because of the smaller density.

Our observations of network events with associated red shifts in the O V and He I lines would not seem to fit in with either of these two models very readily. The strong tendency for periodicity, apparent in Figs. 2 and 3, would seem to demand a regular nanoflare frequency, but the chaotic nature of magnetic reconnection argues against this occurring. The observed periodicity would seem to support the spicular rebound concept, but the difficulty here is that blue-shifted transition region lines are predicted whereas our observations clearly show red shifts.

Our view is that the very large number of network events we observe, together with their apparent periodicity, points to a spicular rebound concept. However present models are missing some important ingredient that if included would give rise to red-shifted transition region lines. This might be the magnetic field. In the models of Hansteen & Wikstøl (1994) and Cheng (1992a, b, c) the magnetic field forms a flux tube which is sim-
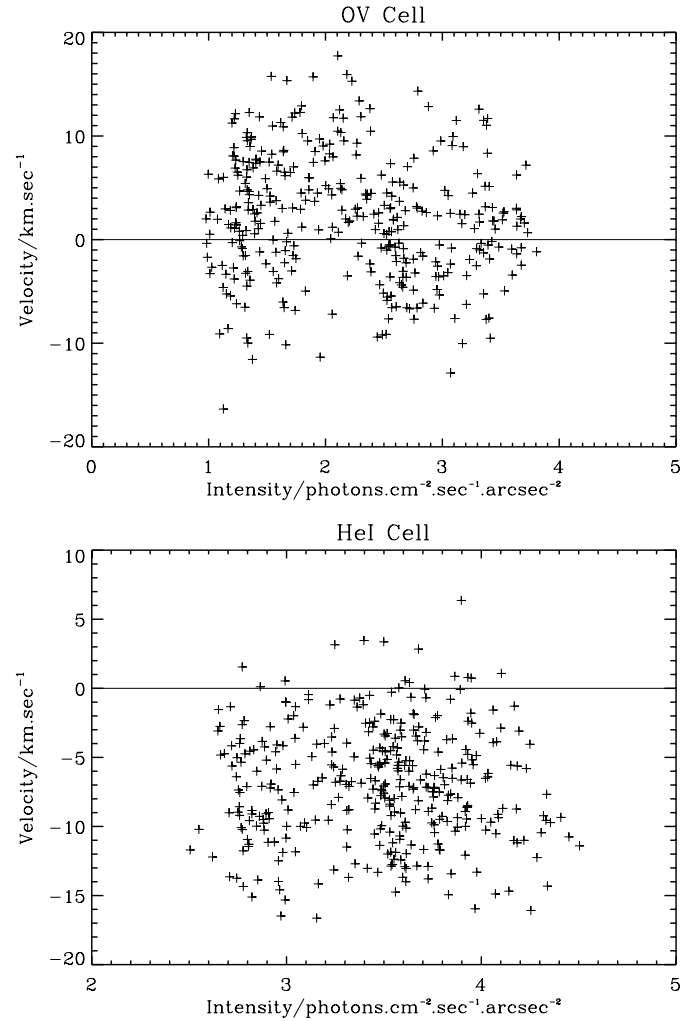
ply a conduit through which the material flows upwards and downwards. A field strength varying with height might lead to different results from those obtained in the present theories.

5.2. Internetwork features

It is widely held that photospherically-generated acoustic waves which propagate upwards and turn into shocks are responsible for the heating of the internetwork chromosphere (Carlsson, Judge, & Wilhelm 1997). The evidence for this is the presence of strong oscillations with period ~ 3 minutes in chromospheric lines, including those seen in the wavelength range of the SOHO/SUMER instrument, which are associated with oscillations in the familiar Ca II grains. Variations in velocities of chromospherically formed N I and C II lines appear to be correlated with intensity variations but with a slight phase lag. There is, however, no such correlation for more highly excited ions (e.g. C III) formed in the transition region, so the shocks would

not appear to be responsible for heating of regions higher than the chromosphere in the internetwork region.

Our findings as discussed are somewhat different. Although there is no evidence in our data for a correlation of velocity and intensity in the O V and He I lines, our preliminary wavelet analysis suggests the presence of a 3-minute oscillatory pattern in both lines over short periods of time (few 1000 s). This result would indicate, contrary to the findings of Carlsson et al. (1997), that acoustic shock heating has some importance up to the level of O V, emitted at 250 000 K, as well as the chromospherically formed He I ion. Furthermore, we find no evidence for highly localised brightenings or flows within the internetwork regions indicating a more subtle heating mechanism occuring in these regions. This is in stark contrast to the nanoflare or spicule like events we find within the network and would seem to suggest that the internetwork chromosphere and transition region are most likely heated via low amplitude acoustic waves generated within the underlying photosphere.

References

Achour H., Brekke P., Kjeldseth-Moe O., Maltby P., 1995, ApJ 453, 945

Andretta V., Jones H.P., 1997, ApJ 489, 375

Arnaud M., Rothenflug R., 1985, A&A 60, 425

Athay R.G., 1984, ApJ 287, 412

Athay R.G., 1988, ApJ 329, 482

Berghmans D., Clette F., Moses D., 1998, A&A 336, 1039

Baudin F., Bocchialini K., Koutchmy S., 1998, In: Schmieder B., Hoffman A., Staude J. (eds.) Proceedings of the ASPE98 meeting. In press

Carlsson M., Judge P.G., Wilhelm K., 1997, ApJ 486, L63

Carlsson M., Stein R.F., 1997, ApJ 481, 500

Cheng Q.Q., 1992a, A&A 262, 581

Cheng Q.Q., 1992b, A&A 266, 537

Cheng Q.Q., 1992c, A&A 266, 549

Dere K.P., Bartoe J.-D.F., Brueckner G.E., 1983, ApJ 267L, 65D

Doyle J.G., van den Oord G.H.J., O'Shea E., Banerjee D., 1999, A&A, submitted

Doyle J.G., van den Oord G.H.J., O'Shea E., Banerjee D., 1998, Solar Physics 181, 51

Gallagher P.T., Phillips K.J.H., Harra-Murnion L.K., Keenan F.P., 1998, A&A 335, 733

Hansteen V.H., Wikstøl Ø., 1994, A&A 290, 995

Hansteen V., Maltby P., Malagoli A., 1996, In: Bentley R.D., Mariska J.T. (eds.) Magnetic Reconnection in the Solar Atmosphere. Proceedings of a *Yohkoh* conference, Bath, March 20–22, 1996, p. 116

Harrison R.A., 1997, Solar Physics 175, 467

Harrison R.A., Sawyer E.C., Carter M.K., et al., 1995, Solar Physics 162, 233

Hollweg J.V., 1982, ApJ 257, 345

Judge P., Carlsson M., Wilhelm K., 1997, ApJ 490, L195

Judge P., Hansteen V., Wikstøl Ø., et al., 1998, ApJ 502, 981

Mariska J.T., 1988, ApJ 334, 489

McClymont A.N., 1989, ApJ 347, L47

Porter J.G., Moore R.L., Reichmann E.J., Engvold O., Harvey K.L., 1987, ApJ 323, 380P

Preś P., Phillips K.J.H., 1999, ApJ 510, L73

Schrijver C.J., Title A.M., Harvey K.L., et al., 1998, Nat 394, 152

Sterling A.C., Hollweg J.V., 1988, ApJ 327, 950

Sterling A.C., Mariska J.T., 1990, ApJ 349, 647

Summers H.P., 1994, Atomic Data and Analysis Structure User Manual. Joint European Torus Publication JET_IR(94)06

Teriaca L., Banerjee D., Doyle J.G., 1999, A&A, submitted

Ulmschneider P., Priest E.R., Rosner R., 1991, Mechanisms of Chromospheric and Coronal Heating. Proceedings of the International Conference, Heidelberg, 5–8 June 1990, Springer-Verlag, Berlin-Heidelberg-New York

Ulrich R.K., 1996, ApJ 465, 436